An electroabsorption modulator-based network architecture for particle physics applications

2011 JINST 6 C12012

(http://iopscience.iop.org/1748-0221/6/12/C12012)

PUBLISHED BY IOP PUBLISHING FOR SISSA

RECEIVED: *November 15, 2011*
ACCEPTED: *November 19, 2011*
PUBLISHED: *December 6, 2011*

TOPICAL WORKSHOP ON ELECTRONICS FOR PARTICLE PHYSICS 2011,
26–30 SEPTEMBER 2011,
VIENNA, AUSTRIA

2011 JINST 6 C12012

An electroabsorption modulator-based network architecture for particle physics applications

S. Papadopoulos,[a,b,1] **I. Darwazeh,**[b] **I. Papakonstantinou,**[b] **J. Troska**[a] **and F. Vasey**[a]

[a] *CERN — European Organization for Nuclear Research, PH Department, CERN CH 1211, Geneva 23, Switzerland*

[b] *Department of Electronic and Electrical Engineering, University College London, Torrington Place, London, WC1E 7JE, U.K.*

E-mail: spyridon.papadopoulos@cern.ch

ABSTRACT: The forthcoming increase in rate of data production and radiation levels, associated with the transition to High-Luminosity Large Hadron Collider, necessitates a readout link upgrade. Such upgrade is also an opportunity to move to a more efficient network infrastructure through the introduction of new technologies and it is in light of this that we explore the possibility of using a unified optical network architecture based on using Reflective Electroabsorption Modulators at the detector side. We evaluate the performance of the new architecture and investigate the way operating and environmental parameters such as wavelength and temperature affect it.

KEYWORDS: Optical detector readout concepts; Radiation-hard electronics; Data acquisition concepts

[1] Corresponding author.

doi:10.1088/1748-0221/6/12/C12012

Contents

2011 JINST 6 C12012

1 Introduction

The evolution of experimental physics has always been coupled with engineering and technological advances. Optical fiber communication technologies are prominent examples as they facilitate the transfer of the large volumes of data generated by particle physics experiments. The Large Hadron Collider (LHC), the world's largest and most powerful particle accelerator, started routine operation in 2009. Two counter-rotating beams of particles are brought into collision at four points around its 27 km circumference. Each collision point is surrounded by special detectors, called "experiments", designed to detect and reconstruct what happens during the collisions [1]. The planned luminosity upgrade of the LHC to High-Luminosity LHC (HL-LHC) will result in increased rate of data production, as well as higher radiation levels. Such increases bring new and challenging design requirements for the data links and their components.

Many types of optical links are in use in the LHC experiments, as currently different types of information are carried over different physical links, developed by different teams. The forthcoming upgrade provides an excellent opportunity to upgrade and consolidate the current network infrastructure to a more efficient and flexible single one that can transport all types of data [2].

Electroabsorption modulators (EAMs) have long been of interest to the particle physics community due to their potential radiation hardness, as well as their low mass and power consumption [3]. Their use was suggested and investigated for the LHC [4], but difficulties related to the immaturity of the technology at the time led to the implementation of different types of optical links based on directly modulated lasers [5, 6]. Recently, EAM technology has reached sufficient maturity and devices are now commercially available. It is therefore timely to revisit the use of EAMs for high-energy physics experiments with a proposal for a new network architecture based on the use of Reflective EAMs (REAMs) [7].

This paper is structured as follows; section 2 briefly describes the proposed network architecture. Section 3 provides the background on operating principles of an EAM that is required

Table 1. Requirements for the upgraded optical links.

Quantity	Value
Upstream Data Rate	10 Gb/s (per user)
Downstream Data Rate	$<$ 1 Gb/s (broadcast)
Link Length	$<$ 1 km
Splitting Ratio	1:16 (target)

to appreciate aspects related to its impact on network performance. As parameters that have an impact on system performance are strongly influenced by the characteristics of the REAM, in section 4 we investigate how these characteristics vary with external parameters, namely wavelength and temperature. Finally, in section 5 we report on our measurements of the quality of the received modulated signal as a function of its power.

2 Network architecture

Although different experiments and sub-detectors may have different bandwidth requirements, a superset of currently available requirements has been collated into the values given in table 1. These values have been used as a conservative estimate of the performance needed from our newly proposed network architecture. In contrast to commercial network applications where greater bandwidth is typically required in the downstream direction, our application requires greater bandwidth in the upstream direction. In the downstream direction most information can be broadcast and hence resources — fiber and transceivers — can be shared. In the upstream direction, however, the high data rate requirement per user makes multiplexing much more challenging. Such "unusual" network requirements led to the design of the architecture depicted in figure 1(a). A splitting ratio of 1:16 or greater has been estimated to be sufficient in order to achieve cost reduction through downstream transmit component sharing.

The downstream transmitter as well as the CW (continuous-wave) optical source, which provides the light to be modulated by the REAM for upstream transmission, are shared. These two components are located in the "counting room", which is an environment set away from the high radiation environment of the detector and is shielded from radiation. An upstream/downstream pair use the same fiber with information being separated using different wavelengths as illustrated in figure 1(a). The wavelength used for upstream transmission will be in the 1520-1560 nm window where REAMs, optical transmitters and receivers are commercially available. The downstream wavelength in this example is chosen to be 1490 nm mainly to explore the possibility of extending the work presented in [2].

3 Electroabsorption modulator

In order to evaluate the impact of different factors affecting the upstream performance, some understanding of the operation of the EAM is required. As figure 1(b) shows, an EAM modulates light using the variation of the absorption of its semiconductor material when an external electric field

2011 JINST 6 C12012

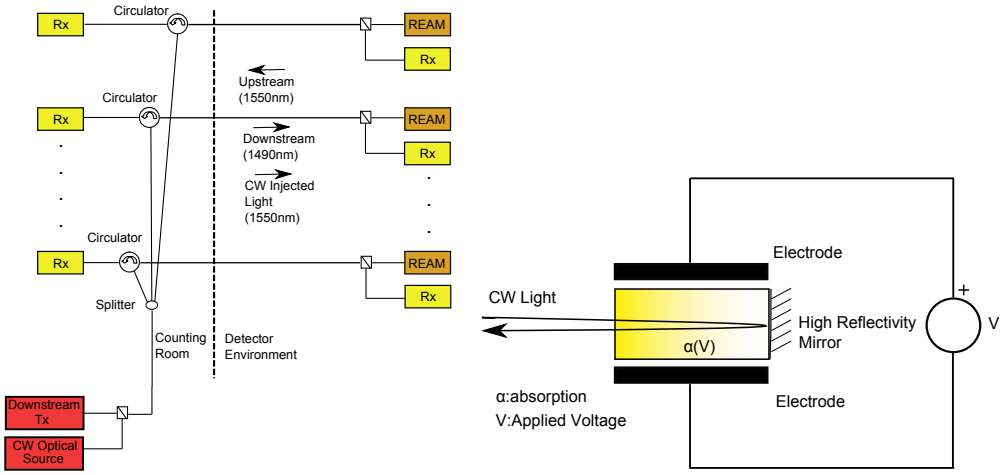

(a) (b)

Figure 1. (a) Network architecture and (b) Simple representation of REAM functionality.

is applied, caused either by the Franz-Keldysh Effect (FKE) or by the Quantum Confined Stark Effect (QCSE) [8]. The EAM used in this work is based on QCSE.

The main metric used to characterize EAMs is their static response, also known as transmission characteristic, switching curve [9] or transfer function [8]. The static response, $T(V)$, is defined as the ratio of the output light intensity over the input light intensity as a function of voltage [9]:

$$T(V) = \frac{P_{\text{out}}(V)}{P_{\text{in}}} \tag{3.1}$$

The generic shape of static response of a QCSE-based EAM at a fixed wavelength is depicted in figure 2. The static response initially decreases with increasing reverse bias voltage until reaching a minimum and then starts increasing. The shape of the static response and its minimum transmission point depend on the structure of the particular device, as well as operating parameters such as wavelength and temperature [9].

The extinction ratio (ER), a parameter that can significantly affect system performance, is defined as the ratio of the optical power at the space (binary "0") level to the power at the mark (binary "1") level [10]:

$$ER = \frac{P_0}{P_1} \tag{3.2}$$

As figure 2 shows, the extinction ratio at DC is determined by the shape of the static response as well as the choice of the operating voltages V_H and V_L and is given in dB by $ER|_{\text{dB}} = T(V_L)|_{\text{dB}} - T(V_H)|_{\text{dB}}$. Therefore, the shape of the static response and the choice of the operating voltages have a direct impact on network design, as they determine the extinction ratio and the associated power penalty [10]:

$$\alpha_{\text{ER}} = 10\log_{10}\frac{1+ER}{1-ER} \tag{3.3}$$

2011 JINST 6 C12012

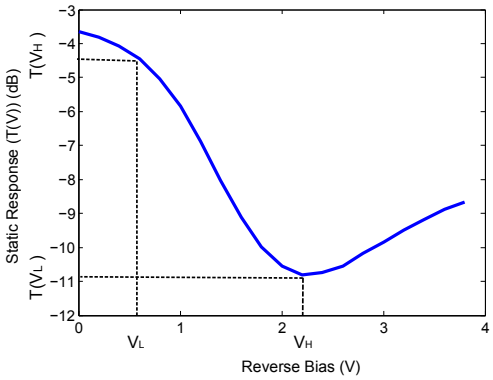

Figure 2. Measured EAM static response and operating voltage (1550 nm).

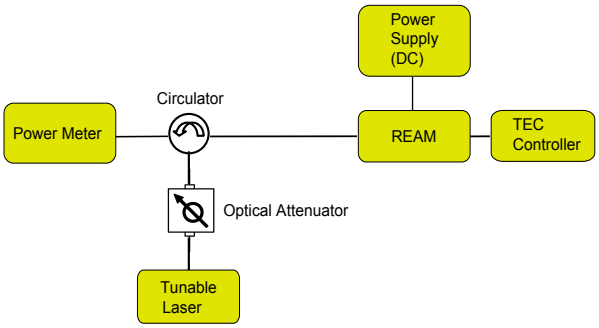

Figure 3. Measurement setup.

4 Static measurements

For the architecture described above, the operating wavelength can be chosen by the network designer, while the operating temperature is not necessarily subject to design decisions unless special measures such as the use of a thermoelectric cooler component are taken. Firstly we evaluate the impact of wavelength and optimize our selection. Subsequently we investigate the impact of temperature on system performance.

The setup that was used to measure the static response of an InP-based, commercially available REAM [11] at different operating conditions is shown in figure 3. A tunable laser diode was used to inject light into the modulator. As the output optical power of the laser could be varied between 6 dBm and 9 dBm and we were interested in the performance of the system at lower power levels, the output power of the laser was arbitrarily set to 7 dBm and a variable optical attenuator was connected to the output of the laser, to set the optical power of the light injected to the system to be 0 dBm. The light was then routed to the REAM via a circulator. After being absorbed and reflected by the REAM, the light was subsequently routed to an optical power meter.

In order to measure the impact of the wavelength of the injected light on the operating characteristics of the REAM, the output wavelength of the tunable laser was varied between 1510 nm and 1640 nm. The REAM bias voltage was varied between 0 V and 3.8 V and the static response was calculated at each wavelength from the power measured at the output of the circulator by taking

2011 JINST 6 C12012

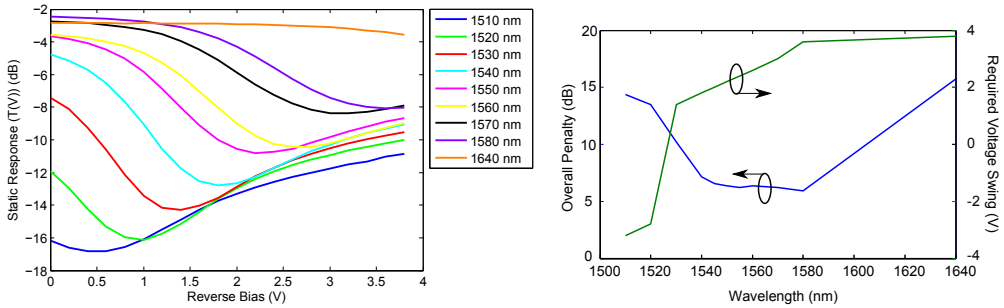

(a) (b)

Figure 4. (a) Static response as a function of wavelength and (b) Overall induced penalty due to insertion loss and imperfect extinction ratio vs. wavelength (left axis) and required voltage swing vs. wavelength (right axis).

into account the connector- and circulator-induced losses at the particular wavelength. The results of the measurements are shown in figure 4(a) and clearly show that care is needed when choosing a bias voltage-wavelength combination to achieve optimum performance in terms of minimizing the insertion loss of a device and maximizing its extinction ratio. To determine the optimum operating wavelength range we calculated the required voltage swing to achieve the maximum extinction ratio (shown in 4(b), right axis) as well as the overall power penalty associated to the extinction ratio and the insertion loss (4(b), left axis), both as a function of wavelength. Both the required voltage swing and the overall penalty should be minimized, we have therefore selected the operating wavelength range to be in the 1550 nm region.

The selection of the modulation voltage levels is more challenging in a temperature-varying environment as the static response is temperature-dependent. Typically the effects of temperature variation are compensated using a thermo-electric cooler (TEC), but for our application this is not acceptable, as it would increase the mass and the power consumption of the front-end component.

The same measurement methodology that was used to investigate the impact of wavelength on static response was also utilized to investigate the impact of temperature variation. The static response at 1550 nm was measured at three different temperatures (10 °C, 30 °C and 50 °C) and the results are shown in figure 5(a). The temperature range of 40 °C has been selected to approximate the maximum temperature difference inside the detector [6]. Figure 5(a) reveals a number of important trends with increasing temperature, namely increase of the insertion loss, decrease of the reverse bias voltage level at which the static response minimum occurs and a slight increase of the maximum extinction ratio.

To assess the impact of temperature it has been assumed that the modulation voltage levels are determined by the static response at the highest operating temperature. The reason is that the static response minimum occurs at low voltage levels when the operating temperature is high. Operation at higher voltages would require the use of both the decreasing and the increasing parts of the static response, leading to significant non-linear effects. The modulation voltage levels were thus set to $V_L = -0.8$ V, $V_{H,\mathrm{Fixed}} = 1.6$ V to maximize the extinction ratio at the highest temperature, as shown in figure 5(a). The obvious problem encountered in this case is the sub-optimum choice of voltage levels at lower temperatures — the optimum at 10 °C, $V_{H,\mathrm{Opt}} = 3$ V is also shown in figure 5(a)

2011 JINST 6 C12012

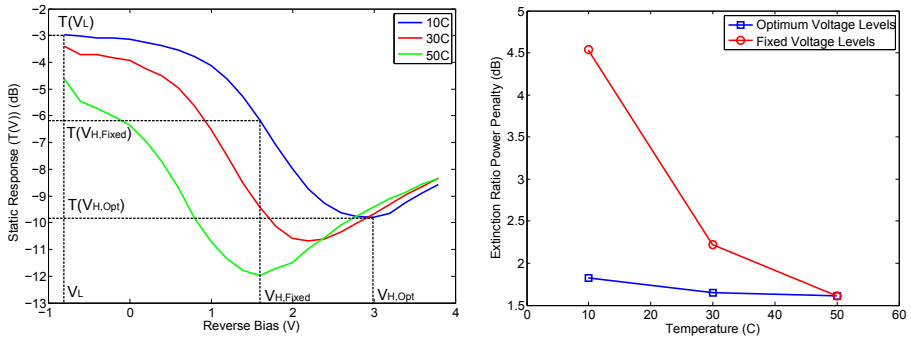

(a) (b)

Figure 5. (a) Temperature Dependence of Static Response and (b) Extinction Ratio Power Penalty Vs. Temperature, for λ=1550 nm.

— leading to a decrease of the extinction ratio. Figure 5(b) shows the calculated extinction ratio power penalty for different temperatures, both when the modulation voltage levels are fixed and when optimum voltage levels are used. Referring back to the architecture shown in figure 1(a), the additional power penalty results in a decrease in the number of users that can share a single downstream transmitter/CW source combination by a factor of ≈ 1.8. This indicates that some voltage adaptation mechanism is required to avoid significant performance degradation.

5 Dynamic measurements

Although static measurements can provide valuable information regarding the performance boundaries of the system and allow us to select optimum values of operating parameters with reasonably good accuracy, dynamic measurements are required to validate the feasibility of the system. We focus on upstream performance, as simple link budget calculations using commercial component values show that the maximum number of users that can be served using the architecture of figure 1(a) is determined by the upstream performance constraints. Figure 6 shows the setup used for the measurements. The setup is similar to the one used for the static measurements, but with a pseudo-random binary sequence (PRBS) source and a wideband amplifier being used to generate a 2^7-1, 10 Gb/s PRBS data stream and modulate the voltage applied to the REAM. Additionally, a 10 Gb/s PIN photodiode receiver with a pre-amplifier was used instead of a power meter to receive the modulated light. The output of the receiver was connected to a digital communications analyzer (DCA) to view and further analyze the received waveform.

The average optical power at the input of the receiver was modified by changing the optical attenuation at the output of the tunable laser. The quality of the signal was measured using the value of Q, a commonly used indicator for the quality of a modulated signal. Q is defined as the ratio of the optical power difference between the mark (I_1) and space (I_0) levels to the summation of the standard deviation (rms values) of noise at the mark (σ_1)and space (σ_0) levels [10]:

$$Q = \frac{I_1 - I_0}{\sigma_1 + \sigma_0} \tag{5.1}$$

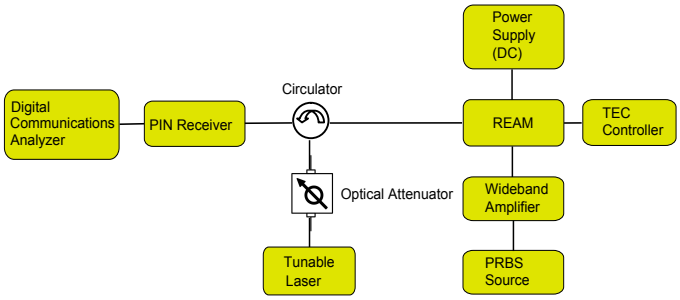

Figure 6. Dynamic measurement setup.

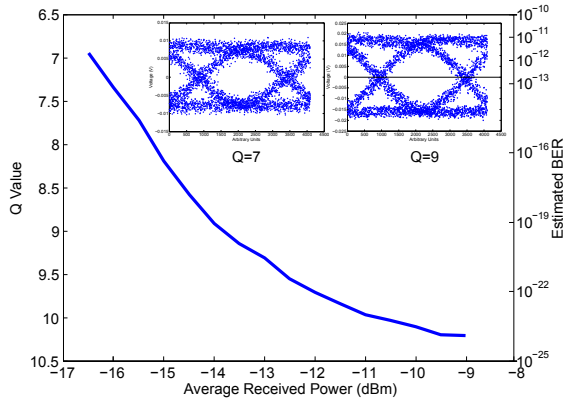

Figure 7. Q-Value and corresponding BER Vs. average received power — eye diagrams for Q=7 and Q=9 (inset).

For noise-limited systems, such as ours, Q determines the bit error rate (BER), equation 5.2 [10]:

$$BER = \frac{1}{2}\mathrm{erfc}\left(\frac{Q}{\sqrt{2}}\right) \approx \frac{\exp\left(-\frac{Q^2}{2}\right)}{Q\sqrt{2\pi}} \tag{5.2}$$

where $erfc$ is the complementary error function.

The plot in figure 7 shows the value of Q — left axis — and the corresponding estimated BER — right axis — as a function of the average received optical power. The recorded eye diagrams for Q = 7 ($BER = 10^{-12}$) and Q = 9 ($BER = 10^{-19}$, that is error-free) are also shown in the inset of the figure. As the diagram shows, the required average power to achieve a BER of 10^{-12} is -16.4 dBm. Referring back to the architecture of figure 1(a), the results suggest that a 10 dBm DFB laser can serve 16 users. Furthermore, measurements of the receiver's thermal noise and comparison against the specifications of other commercial receivers indicate that a splitting ratio of 1:32 could be achieved with the use of a higher sensitivity receiver. Even without this improvement the architecture appears to be cost-efficient in comparison to a point-to-point configuration using REAMs where one cheap low power laser is used as a CW optical source per REAM. Additional cost reduction compared to a point-to-point architecture is achieved due to the downstream transmitter sharing.

2011 JINST 6 C12012

6 Summary

We propose a new network architecture for the bidirectional transfer of information in high energy physics experiments. The architecture is based on the use of commercially available REAMs illuminated remotely by a DFB laser. The wavelength-dependent operation of the REAM has been studied and we have found that the optimum operating wavelength is in the 1550 nm region. The impact of temperature variation on REAM operation has also been investigated and we find that the penalty associated with a 40 °C temperature change can be kept below 0.3 dB with optimum drive voltage settings. The feasibility of the suggested network architecture is demonstrated through measurements of the quality of the received modulated signal at 10 Gb/s as a function of its power.

Acknowledgments

This work was supported in part by ACEOLE, a Marie Curie mobility action at CERN, funded by the European Commission under the 7th Framework Programme. The dynamic response measurements were carried out at UCL with the help of Dr Manoj Thakur for which we are grateful.

References

[1] G. Kane and A. Pierce, *Perspectives on LHC physics*, World Scientific, Singapore (2008).

[2] I. Papakonstantinou et al., *A fully bidirectional optical network with latency monitoring capability for the distribution of timing-trigger and control signals in high-energy physics experiments*, *IEEE Trans. Nucl. Sci.* **58** (2011) 1628.

[3] C. Da Via et al., *Lightwave analogue links for lhc detector front-ends*, *Nucl. Instrum. Meth.* **A 344** (1994) 199.

[4] A. Baird et al., *Analog lightwave links for detector front-ends at the LHC*, *IEEE Trans. Nucl. Sci.* **42** (1995) 873.

[5] G Aad et al., *The ATLAS experiment at the CERN LHC*, 2008 *JINST* **3** S08003.

[6] R. Adolphi et al., *The CMS experiment at the CERN LHC*, 2008 *JINST* **3** S08004.

[7] S. Papadopoulos et al., *A network architecture for bidirectional data transfer in high-energy physics experiments using electroabsorption modulators*, in proceedings of 16th *European Conference on Networks and Optical Communications*, July, 20–22, Northumbria University, U.K. (2011).

[8] G. Li and P. Yu, *Optical intensity modulators for digital and analog applications*, *J. Lightw. Technol.* **21** (2003) 2010.

[9] G. Ghione, *Semiconductor devices for high-speed optoelectronics*, Cambridge University Press, Cambridge U.K. (2009).

[10] G.P. Agrawal, *Fiber-optic communication systems*, 3rd edition, Wiley, New York U.S.A. (2002).

[11] *Reflective Electroabsorption Modulator type EAM-R-10-C-7S-FCA* manufactured by CIP Photonics Ltd., U.K, see http://www.ciphotonics.com.

2011 JINST 6 C12012